Automatic Evaluation of the Mechanical Properties of Steels Maraging using Digital Image Processing Techniques

Angélica Alves Viana*, Savio Lopes Rabelo*, José Daniel de Alencar Santos*,
Venceslau Xavier de Lima Filho*, Douglas de Araújo Rodrigues†,
Roberto Fernandes Ivo† and Pedro Pedrosa Rebouças Filho*

*Instituto Federal de Educação, Ciência e Tecnologia do Ceará, Fortaleza, CE, Brazil
†Universidade Federal do Ceará, Fortaleza, CE, Brazil

***Abstract*—Some strategic sectors of the economy require that the raw material of their machines and equipment have mechanical properties that satisfy their use. Maraging steel is a material of great concern since it is necessary to have a high mechanical resistance associated with high fracture toughness. The traditional tests to determine the fracture toughness of this material before use in applications are the Charpy and K_{IC} tests. However, this process is characterized by being exhaustive and requiring specialized and trained professionals. Thus, to reverse this situation, this work proposes a new approach to determine the mechanical properties of maraging steel. For this, initially, the method removes any artifacts present in the image resulting from the mode of acquisition. In sequence, this works tested the method Extended Minimum Transformation (EMT) and mathematical morphology to find these markers of the regions of the dimples. Then, the Adaptive Thresholding, Optimal Global Thresholdusing the Otsu Method and Watershed transformation methods were used to segment the dimples. In the end, the diameter of the dimples and the toughness of the material were calculated. Tests are carried out and compared with the result obtained by specialists using the traditional system to evaluate the proposed approach. The results obtained were satisfactory for the application because the proposed approach presented speed and precision to the conventional methods.**

I. Introduction

High-performance industries, such as transportation, nuclear, military, petrochemical, and aerospace, require optimized alloys with high mechanical strength and fracture toughness at the same time [1]. Therefore, there is an endless search for alloys that have these properties. These industries have turned their attention to Maraging steels.

Steel Maraging is a class of steel that has the right combination of mechanical strength and tenacity. This steel is considered ultra-high-strength steel with particular non-deformity properties during aging hardening, good weldability, and other characteristics that make it ideal for countless applications.

Due to the critical applicability of this type of steel, many researchers study the mechanical properties of this material. The studies subject steel to tests to assess or improve its strength and toughness characteristics. In [2], samples of Maraging 18Ni class 300 steel were subjected to different solubilization temperatures and the aging procedure. The objective was to evaluate the mechanical properties of this material through the application of these tests and to find a combination of heat treatments that improve its toughness.

Due to the critical applicability of this type of steel, many researchers study the mechanical properties of this material. The studies subject steel to tests to assess or improve its strength and toughness characteristics. Researchers at work [2] subjected Maraging 18Ni class 300 steel samples to different solubilization temperatures and aging. The objective was to evaluate the mechanical properties of this material through the application of these tests, and to find a combination of heat treatments that improve it is toughness.

Toughness is considered the resistance that the material offers to the nucleation or propagation of a crack. In short, it is all the energy that it stores from the first moment when the stresses are applied until the moment when the fracture suffers. The inverse relationship between strength and toughness, well understood for other high-strength steels, is also seen in the 18% Ni Maraging steel family. New studies promote an increase in fracture toughness without considerable losses in mechanical strength. An area of high relevance in the researches is the study that aims to increase the austenite grain, interfering in the micromechanism of crack propagation through the hierarchical structure of the martensitic phase.

There are several ways to measure a material's fracture strength by performing mechanical tests. Tests can have dynamic characteristics, for example, Charpy and K_{IC} tests, or static tests, such as traction [3]–[5].

In Charpy's test, a prismatic bar with a notch in the middle is placed in a device known as a hammer. This device has an articulated arm and a weight at the end of the arm. This weight will be launched against the sample. The stick will transfer energy to the sample. Consequently, this energy will be accumulated in the form of deformation before fracture.

The K_{Ic} test is the most used form, and there is a prismatic bar with a notch in the middle. After a fatigue cycle, the machine applies to bend force to this specimen. Due to the movement, a crack is generated that will propagate up to a certain length. Then, on the same machine, but with a different

configuration, the sample is supported by two points, and a third support point flexes that sample. This flexion will provide energy with the nucleated crack. The amount of energy that the specimen absorbs in this second stage of the test will be the fracture resistance. This test is quite complex, as there are several requirements that it must meet to be a valid test and, therefore, the probability of failure is very high. The K_{Ic} test, in addition to measuring only the crack propagation energy, is still standardized by several associations of technical standards, such as the American Society for Testing and Materials (ASTM) and British Standards Institution (BSI), among others. The main disadvantages of these techniques and the KICs, in particular, are the complexity of the tests, complex validation protocols, and the high associated costs.

There are many fields of application in mechanics and metallurgy that require quantitative and qualitative analysis, both in a scientific study in the laboratory and industrial processes. Quantitative analysis carried out principally by manual methods, for the definition and evaluation of parameters such as grain size, porosity, second phase particles, wear particle morphology, granulometric distribution of inputs or determination of mechanical properties, requires obtaining accurate data and representative to allow the use of statistical concepts, limiting the application of manual methods in the industrial routine, being extremely dependent on the skill of the responsible technician. On the other hand, the complexity of the microstructures of the materials implies the need to characterize quantitatively numerous parameters that cannot or are difficult to be assessed by manual methods, such as spatial distribution, size, volumetric fraction and precipitate morphology, contiguity, etc [6].

More recently, the rapid development of electronics and information technology has enabled the creation of systems based on digital image processing techniques for microstructural evaluation. This scenario has become real recently, due to the application of digital image processing techniques, which allow the automation of these processes, significantly reducing execution times and decreasing errors and improving the reproducibility of measurements.

There is an increasing number of researches that employ computational techniques in several fields of Materials Science to assist professionals and specialists in their analytical activities. There are in the literature, studies that used computational methods to analyze the microstructure of the cast iron [7], [8], calculate the graphite density nodules [9], classify the electric steels according to the electromagnetic efficiency [10]–[12], and measures the welding dilution [13].

Given the above, it is possible to note that the toughness is an essential mechanical property in the evaluation of the resistance of a material. However, the existing ways of calculating it involve testing, which, in addition to presenting high cost, are quite complicated, and there is a high risk of failure. Given the relevance of toughness in mechanical properties in the evaluation of Steel Maraging 18Ni C300, this article aims to use Digital Image Processing (DIP) techniques in the images obtained in the experiments of [2] to extract the average diameters of dimples and to find the values resistance. Therefore, a method in a simple, less stressful, and much cheaper way.

A. Paper organization

Section II deals with the mechanical properties of maraging steels; Section III provides details of the methodology and describes the proposed technique. In Section IV, the results obtained are displayed; Section V presents the conclusions, as well as suggestions for future work.

II. Mechanical Properties of the Maraging Steels

Maraging steels are alloys formed mainly by the chemical elements iron, nickel, molybdenum, and cobalt. The most used designation for these steels informs the nominal nickel content and the minimum value of the stress limit in the tensile test, measured in Megapascal (MPa), in the International System, or kilogram-force per square inch (kpsi), more used in the United States of America (USA) [14]. The stress limit is the stress necessary to produce a small amount of plastic deformation, in which the material does not return to its original state.

The term Maraging comes from the combination of the two English words *mar*tesine and *aging*, which respectively mean martensite and aging, that is, aged martensite. The term already suggests what the heat treatments used in this type of steel are.

There is a relative increase in the ductility of the materials after the solubilization treatment. Then the total deformation and the reduction of the area are observed in the tensile test. Consequently, this characteristic reveals its capacity to undergo plastic deformations in the processes of forming and finishing the parts produced with these steels in this condition. Fracture toughness is the ability of a material to resist fracture in the presence of cracks. Therefore, a material can absorb energy by plastic deformation before fracture. Tenacious materials resist the propagation of defects during plastic deformation.

The Maraging steel has a Ni content between 10% and 30%. The use of 13% Ni in the 400 series and 18% Ni in the 200, 250, 300, and 350 series is common. In these types of steel, the carbon concentration is deficient. During cooling, there is austenite to martensite transformation. The latter being known as Ni martensite and has a high density of disagreements and a high content of alloy elements in a robust solution. In this way, it favors the precipitation of intermetallic compounds around the discrepancies causing the material to harden [15].

To evaluate the mechanical strength, ductility, and toughness of a type of steel, many scholars have already carried out some tests with samples of the material, such as hardness, tensile tests, Charpy impact toughness, fracture toughness, and sensitivity to traction notch.

From the analysis of the microstructures visualized by optical and electronic microscopy, some of these studies sought to establish a relationship between them and the mechanical properties of the materials. This is the aim of the work of Koike *et al.* [16]. The authors analyzed the influence of the microstructure on the apparent dynamic fracture toughness of

ABNT 4340 steel from a conventional Charpy impact test. Koike *et al.* [16] concluded that for different heat treatments, these microstructures have different characteristics.

Experimental evidence indicates that in Maraging steels, the mechanical properties as measured by uniaxial tensile tests and the fracture toughness behavior are influenced to different extents by various metallurgical parameters [17].

Acording to [18], the tenacity K_{IC} can be calculated using Equation 1. Where d is the average diameter of the dimple (in μm), σ is the tensile strength (in MPa) and E is the elasticity module (in GPa).

$$K_{IC} = \sqrt{\frac{\sigma\, d\, E}{2}} \tag{1}$$

Table I shows the properties of steel Maraging 300 associated with each test temperature made in [2].

By joining the information from Equation 1 and Table I, it is possible to determine in which range the *dimples* average diameter is for each of the five test temperatures. For this, the variable d from the Equation 1 is isolated and the elasticity module E present in the equation is used as $200GPa$ associated with steel Maraging 18Ni C300.

This method is used as a parameter for evaluating the DIP techniques to calculate the average diameter of the *dimples* in each of the images obtained and provided by the research [19].

III. Material and Methods

This section presents the materials and methods used in the proposed approach. Subsection III-A describes the material used and its mode of acquisition. In Subsection III-B shows the steps of the computational techniques of DIP used to obtain tenacity values. Figure 1 illustrates the methodology adopted in the proposed approach.

A. Materials

This article used the database obtained in the research by [2]. In total, the data set consists of 121 grayscale images of samples from Maraging Steel 18Ni. All images have dimensions of 484 pixels x 712 pixels. Figure 2 illustrates some of the images from the set of images acquired.

In [2], these samples were submitted to temperatures of $820°C$, $860°C$, $1000°C$, $1050°C$, and $1100°C$ in the K_{IC} test. Table II shows the results of the tenacity and average diameter of the dimples obtained in the survey [2]. These values are references in the validation of the results obtained in the proposed approach of this work.

B. Methods

The approach proposed in this work applies the sequencing of some DIP methods to acquire the ideal average diameter of the dimple values. From the value of the diameter and tensile strength and the modulus of elasticity, the toughness value is calculated from Equation 1. Figure 1 shows the computational steps used in this work.

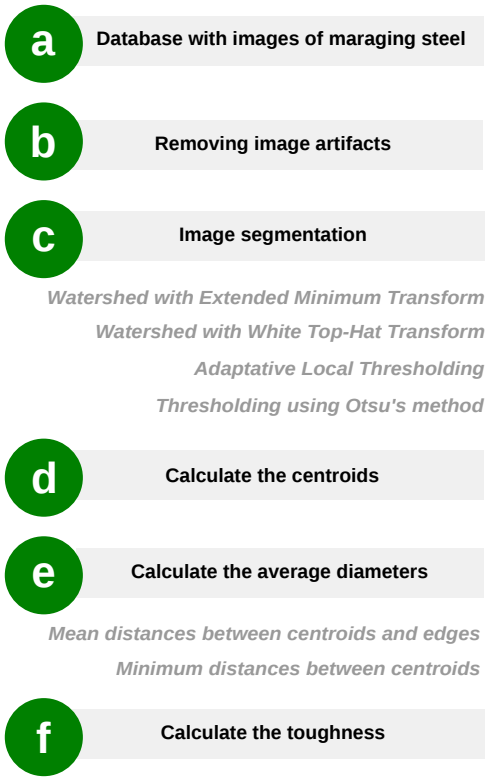

Fig. 1. Diagram illustrating the steps followed until calculating the average diameter dimples in μm.

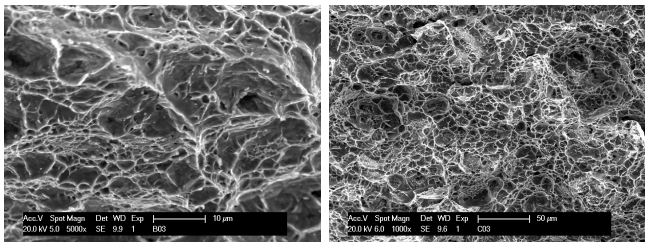

(a) (b)

Fig. 2. Sample images of Maraging Steel 18Ni at temperatures of $860°C$ and $1000°C$, respectively, enlarged by 5000x and 1000x.

As illustrated in Figure 2, the original images have a black region designed to present some information about the conditions and parameters used in image acquisition. However, such areas are considered artifacts that would hinder digital image processing.

There is a standardization of the location of this region with the information. Therefore, initially, for all images in the database, this artifact was removed. In this way, the original images had dimensions of 484 pixels by 712 pixels. With the removal of this region, the image became 423 pixels x 712 pixels.

a) Segmentation of dimples: Some segmentation techniques were tested to obtain dimples segmentations in the image. However, due to the presence of noise and other irregularities, it is necessary to perform pre-processing before

Solution Temperature ($^{\circ}C$)	Tensile Strength (MPa)	Yield Strength (MPa)	Elongation (%)	Necking (%)	Strain Hardening Coef.	Charpy (J/cm^2)	K_{Ic} (MPam$^{1/2}$)	Hardness (HRC)
820	2067±31.6	2052±28.80	9.2±1.07	13.1±2.92	0.18±0.06	15.50	60	54.8
860	1994±75.3	1981±73.75	9.7±0.60	16.2±1.20	0.21±0.05	17.67	65	55.7
1000	1994±75.3	1912±62.40	10.4±0.92	17.5±2.50	0.18±0.03	22.67	76	55.3
1050	1994±75.3	1808±42.60	10.4±0.79	17.8±1.27	0.22±0.02	11.00	78	55.5
1100	1802±86.0	1776±89.70	9.0±0.44	14.7±1.92	0.21±0.02	14.00	83	52.1

TABLE I
MECHANICAL PROPERTIES OF STEEL MARAGING [2].

Temperature ($^{\circ}C$)	Tenacity (MPam$^{1/2}$)	Average Diameter (μm)	Margin (μm)
820	60	17.42	0.27
860	65	21.22	0.80
1000	76	29.99	1.02
1050	78	33.29	1.49
1100	83	38.32	1.83

TABLE II
AVERAGE DIAMETER OF DIMPLES RANGE DIMPLES FOR EACH TOUGHNESS IN THE TEST.

performing the segmentation. If this step is not carried out, there may be over-segmentation, consequently, a large number of targeted regions.

For this, two different methods were tested to find these markers from the regions of the dimples. The first method was based in Extended Minimum Transform (EMT) and the second method was based on mathematical morphology.

The Extended Minimum Transform [20], [21] is a transformation that finds brighter groups of pixels in the image that form connected components whose gray levels are the same. The central markers overlap the locations of the minima with black regions in the original image. This function requires passing a H threshold as a parameter, as can be seen in Expression $m = f_{imextendedmin}(H)$.

In which, m corresponds a binary image that resultants of the application this transform, presenting the regions of local minimums of the original image. This threshold H consists in a factor that be associated a quantity of minimum regions on image. This number of regions and the H factor are inversely proportional, so that the greater this factor, the fewer quantities of minimum regions will be found in the image.

Another way to find the local minimums in an image is to use Morphological Operations. They are digital image processing techniques based on set theory. Often the White Top-Hat (WTH) transform is utilized to extract image components that are brighter than the background in gray-scale image processing [21]. The Expression $T(f) = f - (f \circ b)$ represents this transform. In which, f represents the image, b the structuring element, and $\circ$ denotes the opening operation.

The Figure 3 represents the results of applications of these techniques.

Once the local minimums were found, the next step was to apply segmentation methods to obtain the well-defined dimples. Adaptive Thresholding, Optimal Global Threshold using the Otsu Method, and Watershed transformation methods were tested. Figure 4 shows the results of applying each technique.

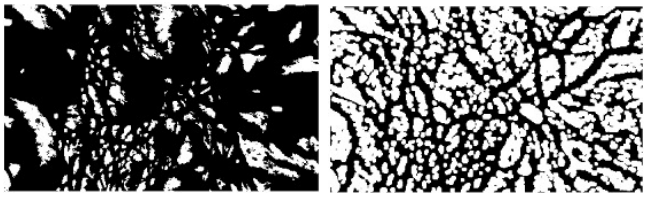

(a) (b)

Fig. 3. Markers: (a) Application of Extended Minimum Transform. (b) Application of White Top-Hat Transform.

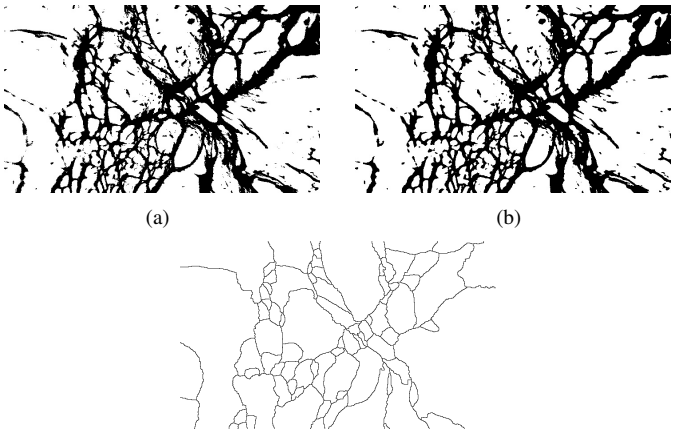

(a) (b) (c)

Fig. 4. Image Segmentation Techniques: (a) Thresholding using T = 127. (b) Optimum Global Thresholding Using Otsu's Method. (c) Watershed Transform.

The Basic Thresholding consists in a segmentation technique that It is necessary a single threshold to segment the object of interest. It is based in the histogram of image. If the grayscale of the pixels background It is so different of the grayscale of the object, this technique is the best to apply.

Suppose that f is the intensity of input image histogram and g is the intensity of output image histogram. The application of the basic thresholding technique is mathematically represented by Equation 2. In which, T represents the single threshold used and the values 1 and 0 are the maximum and minimum intensity of grayscale (black and white colors), respectively.

$$g(x,y) = \begin{cases} 1, \; if \; f(x,y) > T \\ 0, \; if \; f(x,y) \leq T \end{cases} \tag{2}$$

Optimum Global Thresholding Using Otsu's Method determine the optimum threshold k^* to segment the image, through

maximizing the between-classes variance. The algorithm of this method is presented in Algorithm 1.

Algorithm 1 Optimum Global Thresholding Using Otsu's Method.

1: Normalize the histogram of input image;
2: Calculate $P_1(k)$, for k in [0, L-1], using

$$P_1(k) = \sum_{i=0}^{k} p_i$$

3: Calculate the comulative means, m(k), for k in [0, L-1], using

$$m(k) = \sum_{i=0}^{k} ip_i$$

4: Calculate the global intensity mean, m_G, using

$$m_G = \sum_{i=0}^{L-1} ip_i$$

5: Calculate the between-classes variance $\sigma_B^2(k)$, for k in [0, L-1], using

$$\sigma_B^2(k) = \frac{[m_G P_1(k) - m(k)]^2}{P_1(k)[1 - P_1(k)]}$$

6: Find the optimum threshold k^*, as the value of k for that $\sigma_B^2(k)$ is maximum.
7: Obtain the separability measure, η^*, calculating

$$\eta^* = \frac{\sigma_B^2(k)}{\sigma_G^2}$$

Where σ_G^2 is the global variance, defined by

$$\sigma_G^2 = \sum_{i=0}^{L-1} (i - m_G)^2 p_i$$

The Watershed transform [22] is a segmentation method based on mathematical morphology. In this way, an image is considered a topographic landscape with peaks and valleys. The elevation of water in the landscape is represented by the level of gray or the magnitude of the gradient. This transformation decomposes the image in hydrographic basins (regions). For each local minimum, a hydrographic basin comprises all points whose steepest descent trajectory ends at that minimum. One of the approaches to implement this algorithm was proposed by [23].

b) Calculation of centroid and average diameter of dimples: In a two-dimensional image, the centroid of a given the segmented area A corresponds to the point of the A that represents the midpoint at $\tilde{x}$ and $\tilde{y}$. The values are calculated by Equations 3 and 4. Therefore, the centroid of an area is a weighted average of the area's pixels. Consequently, it was calculated the centroid in each microcavity in the segmented image. This centroid represents the microcavity.

$$\tilde{x} = \frac{1}{A} \sum_{(x,y) \in R} x \tag{3}$$

$$\tilde{y} = \frac{1}{A} \sum_{(x,y) \in R} y \tag{4}$$

This work used two different procedures to calculate the radius of each of these regions.

The first procedure disregards the borders that define each region, and the relevant information is only the centroid. The diameter value for each region corresponds to the average of all distances from a centroid to the nearest centroid.

In the second method, the Euclidean distance from the centroid to some edges of the region was calculated. Therefore, this method performs the calculation of several radii. The determination of the average radius and the average diameter was based on the calculation of the average radius of each of these regions.

Equation 5 mathematically expresses the calculation of the radius of each dimple i. The parameter S is the number of selected samples, and $C_i.x$ e $C_i.y$ are the x and y coordinates of the centroid i respectively.

$$R_i = \frac{1}{S} \sum_{j=1}^{S} \sqrt{(x_j - C_i.x)^2 + (y_j - C_i.y)^2}, \tag{5}$$

With the calculation of the radius of each region, the average diameter in pixels is given by Equation 6. In which, N corresponds to the number of regions or centroids in the image. Figure 1 summarizes the steps previously described using a simplified flowchart.

$$DM = \frac{2}{N} \sum_{i=1}^{N} R_i, \tag{6}$$

Figure 5 shows the partial results found until obtaining the average diameter of the dimples for a 1000x magnified image and referring to a temperature test of $1100°C$.

After all the procedures performed to find the average diameter of the dimples in pixels, this value was converted to μm. This conversion was performed by counting the number of pixels of the ruler defined in the black stripe of the original image and obtaining the value of a pixel in μm. Equation 7 describes the relation between a distance in pixels and a distance in micrometer.

$$dm_\mu = dm_p \left(\frac{r_\mu}{r_p} \right) \tag{7}$$

In which, dm_μ and dm_p are the values of the average diameters of dimples in μm, and in pixels, respectively, r_μ and r_p are the values of the ruler in μm and pixels.

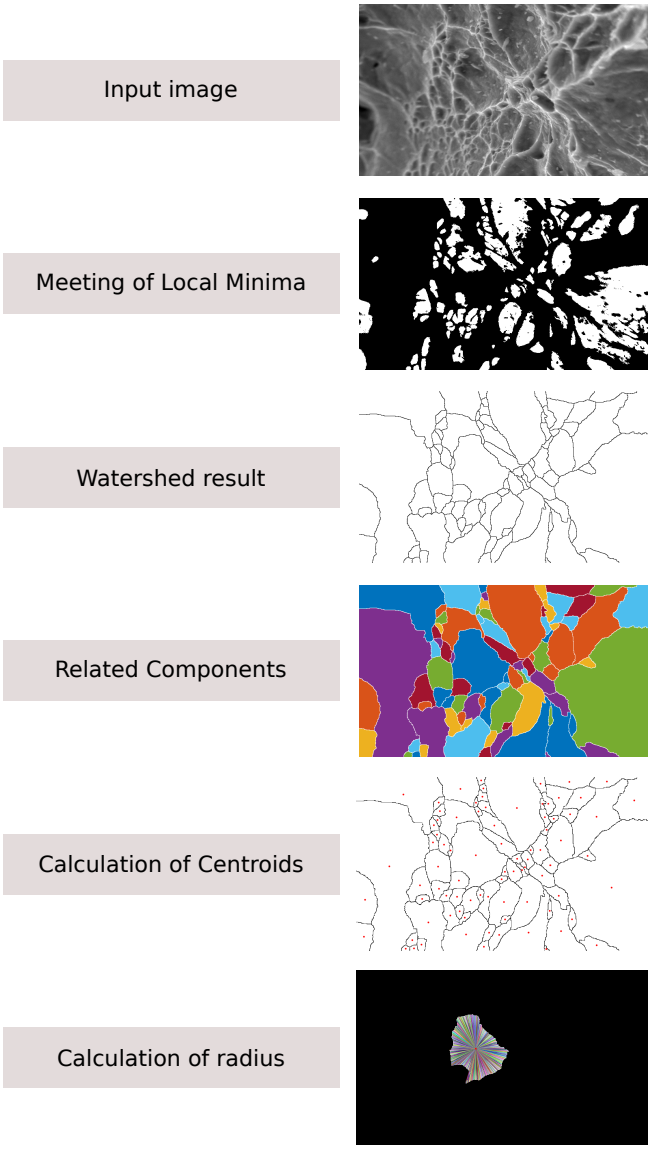

Fig. 5. Step by step to obtain the average diameter of the dimples for an image. (a) Original Image. (b) Meeting of Local Minima. (c) Watershed result. (d) Related Components. (e) Calculation of Centroids. (f) Calculation of radii from the center of a given region.

c) Calculation the tenacity: After that, the tenacity values were found by applying the average diameter values selected in Equation 1, using the most adequate values of average diameters for each image.

The most adequate values of the average diameter chosen for each image were obtained by calculating the Euclidean distance of the average diameters from those found for the ideal average diameter, which would be the closest to the values obtained in Table III according to test temperature value.

C. Experiments

As presented in this section, the approach adopted in this work used different combinations of digital image processing methods to obtain the values of the mechanical properties of toughness in Maraging steel. In total, eight experiments were carried out. Table IV shows the combinations of the DIP methods adopted.

For all the experiments was used a computer with the following configuration: Intel(R) Core(TM) i7-6500U processor with 2.5 GHz, 8 GB of RAM, and running Windows 10. Besides that, It was used the MATLAB 2017a (developed by MathWorks) for implementation.

The parameters used in each DIP algorithm involved in the experiments were selected from the optimization algorithm Grid Search [24], which allows the selection of the best settings from an exhaustive search within a range of predefined values.

For the Extended Minimum Transform, Grid Search was applied with values in the range of 70 to 200 with a step of size 5 to select the parameter H.

For the White Top-Hat Transform, as seen in Section III-B, it is necessary to define the size and shape of the structuring elements used. For experiments with this transform, circles were used. Their sizes were defined from the application of the Grid Search algorithm with combinations of pairs of values. These combinations were: (3; 9), (3; 11), (3; 15), (5; 9), (5; 11), (5; 15), (7; 9), (7; 11), and (7; 15).

The methods Adaptative Thresholding and Optimal Global Threshold using Otsu Method do not require parameters, as both ways are adaptive and adjust their settings automatically according to the image.

All the experiments described above generated estimated values for the average diameter of the dimples, which applied to Equation 1 resulted in toughness values for each image in the database. In the end, the mean and standard deviation of these toughness values, associated with each test temperature, were calculated and subsequently validated with the values found by [2].

IV. Results and Discussion

Table V presented the results of the average tenacities obtained from the experiments described in Subsection III-C and the results of [2].

Table V represents the mean and the standard deviation of the tenacities obtained for each image that refers to a material submitted to a test of a specific temperature. It's possible to observe that the first and second experiments came closer to the values obtained in [2] than the rest.

In both experiments, this works used the technological Watershed Transformation. This method is a powerful tool for image segmentation, which is ideal for targeting regions of gray shades that are not uniform and that are not well defined. Consequently, it is also inversely proportional to the value of the average diameter of the dimples. Thus, applying a grid search with a wide range of benefits, the probability of finding the ideal average diameter of the dimples is higher.

Although this works used two different ways of calculating the average diameters of the dimples, the results varying only those methods did not result in significant variations.

T ($^{\circ}C$)	Real Tenacity ($MPam^{1/2}$)	Estimated Average Diameters(μm)					
		Threshold 70	Threshold 80	Threshold 90	Threshold 92	Threshold 95	Threshold 100
820	17.42	8.29	11.36	17.03	17.15	20.68	29.44
860	21.22	6.39	7.89	11.23	12.03	20.14	20.67
1000	29.99	13.50	24.22	34.66	38.85	46.62	59.66
1050	33.29	12.41	18.41	31.83	36.66	45.78	51.77
1100	38.32	9.83	13.21	19.61	21.02	21.04	23.48

TABLE III
AVERAGE VALUES OF THE AVERAGE DIAMETERS OF THE DIMPLES FOR EACH TEST TEMPERATURE.

Experiments	Find Markers	Segmentation	Calculate
1	EMT	Watershed	Method 1
2	EMT	Watershed	Method 2
3	Morphology	Watershed	Method 1
4	Morphology	Watershed	Method 2
5	-	Thresholding	Method 1
6	-	Thresholding	Method 2
7	-	Otsu	Method 1
8	-	Otsu	Method 2

TABLE IV
THE DIP METHODS THAT WERE USED IN EACH EXPERIMENT.

In experiments 3 and 4, both using mathematical morphology to find the markers, it was necessary to perform a grid search for the sizes of the structuring elements. The small variations in these sizes cause significant changes in the results. Therefore, either the toughness value was far below or far above what was desired.

In experiments that used the Adaptive Threshold or Optimized Global Threshold Using the Otsu Method as segmentation methods, there was no need to find markers or define parameters, as the limits of these methods are set automatically through their algorithms. Thus, as these types of segmentation are ideal for segmenting objects whose gray tone is very different from the gray tone of the image's background, we have poor segmentation, which consequently generates unwanted tenacity values at the end of the algorithm.

Figure 6 shows the box diagrams. These graphics presented that highlight the values corresponding to methods 1 (Figure 6.a) and 2 (Figure 6.b) compared to the traditional way performed in the work of [2]. A black line inside the box symbolizes the average value. The red box corresponds to the toughness test by the traditional method and the black one with the digital image processing methods. Results for temperatures $820^{\circ}C$, $860^{\circ}C$, $1000^{\circ}C$, $1050^{\circ}C$, and $1100^{\circ}C$ are displayed.

An essential factor to note is that the thresholds H and the mean values of the diameters follow a monotonic behavior, the functions that relate the thresholds with the values of the mean diameters of the ripples. Therefore, both grow together. This characteristic allows the analysis to be expanded to limit values beyond the range established in this study.

V. CONCLUSION

Measuring the mechanical properties of maraging steels is generally an exotic process and always requires a specialist to perform the tests, in addition to expensive equipment. To automatically evaluate the mechanical properties of maraging steels, this work developed a system to carry out this analysis automatically using digital image processing methods.

Regarding the technologies used, to find the markers for dimpled regions, the Extended Minimum Transformation (EMT) method, and the method based on mathematical morphology were tested. For segmentation, were used the Adaptive Threshold, Global Optimal Limit transformation methods using the Otsu method and Watershed to segment the dimples. Then the diameter of the dimples and the strength of the material were caculated. The combination of the Watershed with the EMT method showed more significant equivalence with the traditional techniques performed by specialists.

Thus, this article proposes a new automatic approach for calculating the mechanical properties of maraging steel in digital images using sequential digital image processing methods. The main contribution of the developed system is the automatic determination of the toughness of the steel without the need for expensive equipment.

From the validation data of the described approach, it is verifiers that the model is valid, within the allowed tolerance range. Therefore, students, engineers, researchers, and specialists in engineering and materials science can use both at the academic and industrial levels.

REFERENCES

[1] D. Raabe, D. Ponge, O. Dmitrieva, and B. Sander, "Designing ultrahigh strength steels with good ductility by combining transformation induced plasticity and martensite aging," *Advanced Engineering Materials*, vol. 11, no. 7, pp. 547–555, 2009.

[2] V. X. de Lima Filho, "Influência da temperatura de solubilidade nas propriedades mecânicas do aço maraging 300," PhD dissertation, Universidade Federal do Ceará, Fortaleza, Brasil, 6 2018.

[3] W. Server and A. S. Tetelman, "The use of pre-cracked charpy specimens to determine dynamic fracture toughness," *Engineering Fracture Mechanics*, vol. 4, no. 2, pp. 367–375, 1972.

[4] H.-K. Oh, "Determination of fracture toughness by uniaxial tensile test," *Engineering fracture mechanics*, vol. 55, no. 5, pp. 865–868, 1996.

[5] V. Diwakar, S. Arumugam, T. Lakshmanan, and B. Sarkar, "Fracture toughness of maraging steel from charpy "v" notch specimens," *Journal of materials science*, vol. 24, no. 11, pp. 3994–3999, 1989.

[6] I. de Assis do Nascimento, A. R. Soares, and A. L. de Brito Baptista, "A utilização da análise de imagens como ferramenta do ensaio metalográfico no controle de qualidade de peças de ferro fundido: Tubos e conexões," *57 Congresso Internacional da ABM*.

[7] D. d. A. Rodrigues, G. P. d. Santos, M. C. Fernandes, J. C. d. Santos, F. N. C. Freitas, and P. P. Rebouças Filho, "Classificação automatica do tipo de ferro fundido utilizando reconhecimento de padrões em imagens de microscopia," *Matéria (Rio de Janeiro)*, vol. 22, 00 2017.

[8] E. S. Rebouças, A. M. Braga, R. C. Marques, and P. P. R. Filho, "A new approach to calculate the nodule density of ductile cast iron graphite using a level set," *Measurement*, vol. 89, pp. 316 – 321, 2016.

[9] F. d. M. Peixoto and E. Rebouças, "Desenvolvimento de um Software para cálculo da densidade de nódulos de grafita em ferro fundido nodular através de Processamento Digital de Imagens," *Matéria (Rio de Janeiro)*.

Experiments	$820°C$	$860°C$	$1000°C$	$1050°C$	$1100°C$
1	59.30±1.37	67.28±1.76	76.49±4.31	82.54±4.21	83.70±0.88
2	59.58±1.24	67.00±3.31	79.01±1.27	81.09±3.37	84.23±0.45
3	51.16±0.62	49.03±0.65	48.54±4.04	47.58±1.01	47.76±2.78
4	50.40±2.83	55.90±9.18	76.48±13.58	67.52±19.29	85.18±19.33
5	15.82±0.28	16.82±0.28	16.66±0.55	17.21±0.23	16.50±0.65
6	19.68±0.24	19.14±0.25	19.54±1.47	19.55±0.70	18.75±1.07
7	14.28±0.48	15.89±0.57	17.12±1.35	16.62±1.55	15.47±0.61
8	21.49±2.89	18.31±0.47	22.97±7.17	26.13±3.71	17.94±0.92
K_{Ic}	60.87±1.64	66.77±2.91	78.60±2.83	80.89±3.44	82.84±2.27

TABLE V
RESULTS OF ALL EXPERIMENTS.

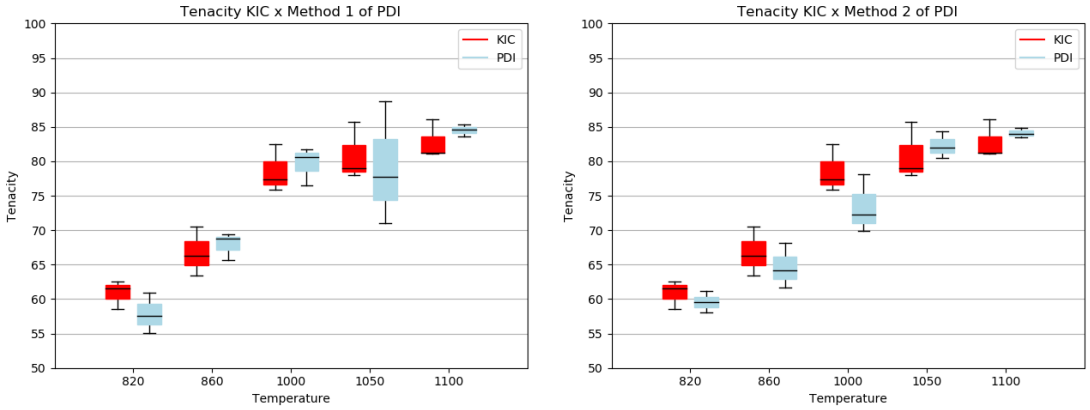

(a) (b)

Fig. 6. Comparative boxplot between the results of [2] and method 1 (a) and method 2 (b) of DIP.

[10] R. F. Ivo, D. de Araújo Rodrigues, J. C. dos Santos, F. N. C. Freitas, L. F. G. Herculano, H. F. G. de Abreu, and P. P. R. Filho, "Study and classification of the crystallographic orientation distribution function of a non-grain oriented electrical steel using computer vision system," *Journal of Materials Research and Technology*, vol. 8, no. 1, pp. 1070 – 1083, 2019.

[11] P. P. R. Filho, J. C. dos Santos, F. N. C. Freitas, D. de Araújo Rodrigues, R. F. Ivo, L. F. G. Herculano, and H. F. G. de Abreu, "New approach to evaluate a non-grain oriented electrical steel electromagnetic performance using photomicrographic analysis via digital image processing," *Journal of Materials Research and Technology*, vol. 8, no. 1, pp. 112 – 126, 2019.

[12] R. F. Ivo, D. de A. Rodrigues, G. M. Bezerra, F. N. Freitas, H. F. G. de Abreu, and P. P. R. Filho, "Non-grain oriented electrical steel photomicrograph classification using transfer learning," *Journal of Materials Research and Technology*, vol. 9, no. 4, pp. 8580 – 8591, 2020.

[13] G. B. Holanda, D. d. A. Lima, and P. P. Rebouças Filho, "Uma nova abordagem para a medição da diluição de soldagem, baseada nos pontos de inflexão de um Contorno Ativo," *Matéria (Rio de Janeiro)*, vol. 24, 00 2019.

[14] M. N. Rao, "Progress in understanding the metallurgy of 18% nickel maraging steels," *Zeitschrift für Metallkunde*, vol. 97, no. 11, pp. 1594–1607, 2006.

[15] J. C. Lopes, "Os aços maraging," *Ciência & Tecnologia dos Materiais*, vol. 19, no. 1-2, pp. 41–44, 2007.

[16] A. Koike, R. Tokimatsu, F. Nogueira, S. Irikura, G. de Caracterização Mecânica, and M. dos Materiais, "A influência da microestrutura na tenacidade à fratura dinâmica aparente do aço abnt 4340," *Anais do 17º CBCIMat–15 a*, vol. 19, 2006.

[17] H. Chandra-Holm, M. Bichsel, and P. Uggowitzer, "The fracture toughness behaviour of a 18 ni (300 grade) maraging steel in various solution treated and aged conditions," *Scripta metallurgica*, vol. 18, no. 4, pp. 373–378, 1984.

[18] H. Stüwe, "The work necessary to form a ductile fracture surface," *Engineering Fracture Mechanics*, vol. 13, no. 2, pp. 231–236, 1980.

[19] V. X. d. Lima Filho, "Influência da temperatura de solubilidade nas propriedades mecânicas do aço maraging 300," Ph.D. dissertation, Universidade Federal do Ceará, Jun. 2018, (visited on 02/03/2020). [Online]. Available: http://www.repositorio.ufc.br/handle/riufc/47921

[20] R. C. Gonzales and R. E. Woods, "Digital image processing," 2002.

[21] P. Soille, *Morphological image analysis: principles and applications*. Springer Science & Business Media, 2013.

[22] A. N. Strahler, "Quantitative analysis of watershed geomorphology," *Eos, Transactions American Geophysical Union*, vol. 38, no. 6, pp. 913–920, 1957.

[23] L. Vincent and P. Soille, "Watersheds in digital spaces: an efficient algorithm based on immersion simulations," *IEEE Transactions on Pattern Analysis & Machine Intelligence*, vol. 1, no. 6, pp. 583–598, 1991.

[24] I. Syarif, A. Prugel-Bennett, and G. Wills, "Svm parameter optimization using grid search and genetic algorithm to improve classification performance," *Telkomnika*, vol. 14, no. 4, p. 1502, 2016.